Methane Monooxygenase Component B Mutants Alter the Kinetics of Steps Throughout the Catalytic Cycle†

Bradley J. Wallar and John D. Lipscomb*

Department of Biochemistry, Molecular Biology, and Biophysics and Center for Metals in Biocatalysis, University of Minnesota, Minneapolis, Minnesota 55455

Received October 2, 2000; Revised Manuscript Received December 18, 2000

ABSTRACT: Component interactions play important roles in the regulation of catalysis by methane monooxygenase (MMO). The binding of component B (MMOB) to the hydroxylase component (MMOH) has been shown in previous studies to cause structural changes in MMOH that result in altered thermodynamic and kinetic properties during the reduction and oxygen binding steps of the catalytic cycle. Here, specific amino acid residues of MMOB that play important roles in the interconversion of several intermediates of the MMO cycle have been identified. Both of the histidine residues in *Methylosinus trichosporium* OB3b MMOB (H5 and H33) were chemically modified by diethylpyrocarbonate (DEPC). Although the DEPC−MMOB species exhibited only minor changes relative to unmodified MMOB in steady-state MMO turnover, large decreases in the formation rate constants of the reaction cycle intermediates, compound **P** and compound **Q**, were observed. The site specific mutants H5A, H33A, and H5A/H33A were made and characterized. H5A and wild type MMOB elicited similar steady-state and transient kinetics, although the mutant caused a slightly lower rate constant for **Q** formation. Conversely, H33A exhibited a >50-fold decrease in the **P** formation rate constant, which resulted in slower formation of **Q**. The kinetics of the double mutant (H5A/H33A) were similar to those of H33A, suggesting that the highly conserved residue, H33, has the most significant effect on the efficient progress of the cycle. Ongoing NMR investigations of residues perturbed by formation of the MMOH−MMOB complex suggested construction of the MMOB N107G/S109A/S110A/T111A quadruple mutant. This mutant was found to elicit a nearly 2-fold increase in specific activity for steady-state MMO turnover of large substrates such as furan and nitrobenzene but caused no similar increase for the physiological substrate, methane. While the quadruple mutant did not have a significant effect on **P** and **Q** formation, it caused an almost 3-fold increase in the decay rate constant of **Q** for furan oxidation and a 2-fold faster product release rate constant for *p*-nitrophenol resulting from nitrobenzene oxidation. Conversely, this mutant caused the **Q** decay rate constant to decrease 7-fold for methane oxidation but left the product release step unaffected. These results show for the first time that MMOB exerts influence at late as well as early steps in the catalytic cycle. They also suggest that MMOB plays a critical role in determining the ability of MMO to distinguish between methane and larger substrates.

Soluble and particulate methane monooxygenases (MMOs)[1] expressed in methanotrophic bacteria are the only enzymes that can efficiently catalyze the oxidative cleavage of the extremely stable C−H bond of methane (*1*−*9*). The soluble form of the enzyme exhibits the following stoichiometry:

$$CH_4 + NAD(P)H + O_2 + H^+ \rightarrow CH_3OH + NAD(P)^+ + H_2O \quad (1)$$

As isolated from *Methylosinus trichosporium* OB3b, the soluble form of MMO consists of three independent protein components: a 245 kDa hydroxylase component (MMOH) having an $(\alpha\beta\gamma)_2$ subunit structure with each protomer containing an active site, a 38 kDa reductase component containing FAD and a $[Fe_2S_2]$ cluster that serves to transfer electrons to MMOH, and a small 15 kDa protein termed component B that has no known cofactors (*1*−*3*, *10*). MMOH contains a non-heme bis-μ-hydroxo-bridged binuclear iron cluster in the active site that has been shown by kinetic and spectroscopic studies to be responsible for catalysis (*10*−*17*).

Single-turnover transient kinetic and spectroscopic studies have led to the proposed mechanism for MMO shown in Scheme 1 (*1*, *10*, *18*−*20*). Molecular oxygen can react with

† This work was supported by National Institutes of Health (NIH) Grant GM-40466. B.J.W. was supported in part by NIH Training Grant GM-07323.

* To whom correspondence should be addressed: Department of Biochemistry, Molecular Biology, and Biophysics, University of Minnesota, 6-155 Jackson Hall, 321 Church St. SE, Minneapolis, MN 55455. E-mail: lipsc001@tc.umn.edu. Telephone: (612) 625-6454. Fax: (612) 624-5121.

[1] Abbreviations: MMO, methane monooxygenase; MMOH, MMO hydroxylase; $MMOH_{act}$, MMOH active sites ($MMOH_{act}$:MMOH ratio of 2); MMOB, MMO component B; MMOR, MMO reductase; MOPS, 3-morpholinopropanesulfonic acid; DEAE, diethylaminoethyl; DEPC, diethylpyrocarbonate; **O**, **P***, **P**, **Q**, and **T**, intermediates **O**, **P***, **P**, **Q**, and **T** from the MMOH catalytic cycle; $\mathbf{H^r}$, diferrous form of MMOH; $\mathbf{H^{ox}}$, diferric form of MMOH; T4MOD, toluene 4-monooxygenase component D.

10.1021/bi002298b CCC: $20.00
Published on Web 01/26/2001

Scheme 1: Proposed Catalytic Cycle of MMOH[a]

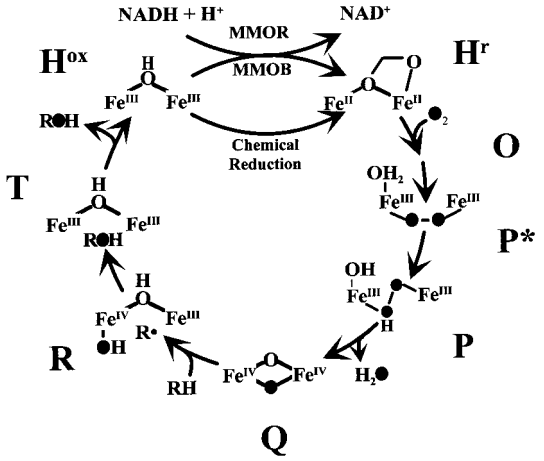

[a] The filled oxygen atoms represent our current understanding of the fate of the atoms derived from O_2. The structures of the intermediates **O** through **T** are based on spectroscopic and model studies.

the reduced form of MMOH [Fe(II)Fe(II)] (**H**^{r}) to form intermediate compound **O**. Because **O** has spectroscopic properties similar to those of **H**^{r}, it is postulated that the associated O_2 is not bound to the binuclear cluster in this intermediate. **O** then decays to compound **P*** with the associated loss of an integer spin EPR signal at $g = 16$ that is characteristic of **H**^{r} (*18*, *21*), suggesting that O_2 is bound to the cluster in this species, resulting in a shift in electron density to yield a diferric [Fe(III)Fe(III)] peroxy or a mixed-valent [Fe(II)Fe(III)] oxy complex. **P*** decays to a different diferric peroxy species, compound **P**, characterized by a weak absorbance at 700 nm (*19*, *22*−*24*). **P** then spontaneously converts to compound **Q**. **Q** is a unique yellow intermediate that has been shown to contain a diferryl-oxo cluster [Fe(IV)Fe(IV)] by Mössbauer studies (*24*, *25*). Additionally, EXAFS experiments have revealed that the O−O bond is broken in **Q** and at least two single-atom oxygen bridges link the irons of the cluster, forming a "diamond core" structure (*24*). **Q** is the form of MMOH that reacts with substrates, and it is the first monooxygenase intermediate to have been trapped and characterized that is capable of reacting directly with unactivated hydrocarbons to yield hydroxylated products. It should be noted that it appears that one proton is necessary in both the **P***-to-**P** and **P**-to-**Q** steps (*19*). After the reaction of **Q** with the substrate, product-bound compound **T** is formed, and with the release of the product, the resting diferric state of MMOH (**H**^{ox}) is regenerated in the rate-limiting step of catalysis (*18*).

Although MMOH in the absence of MMOB is capable of high yields of product formation from both single-turnover and NADH/MMOR-coupled multiple-turnover reactions (*10*, *20*), the rates of these reactions are very low, suggesting that MMOB has a very significant impact on catalysis. Accordingly, transient kinetic studies have revealed two major effects of MMOB on the turnover rate (*20*). First, it causes a 1000-fold increase in the rate of formation of an intermediate **P*** (*18*, *26*). Second, it accelerates the formation of **Q** from **P**, thereby maximizing its formation and preventing uncoupling due to nonproductive breakdown of **P**. These effects on catalysis are very dramatic such that essentially no **Q** accumulates in the absence of MMOB. The detailed mechanism by which MMOB regulates the conversion rates of the reaction cycle intermediates is unknown, but the effect is clearly mediated through the formation of a specific complex with the α-subunit of MMOH (*27*). Spectroscopic studies have shown that this complex alters the environment of the binuclear iron site (*27*−*30*). The conformational changes at the active site of MMOH induced by MMOB binding have other effects on catalysis as well. For example, it has been observed that the regiospecificity of hydroxylation for alternative MMO substrates that are more complex than methane is dramatically altered when MMOB is added (*31*), suggesting that their binding orientation in the active site is changed. Also, the redox potential of the binuclear iron site is changed dramatically when MMOB binds, causing a coupled change in the MMOH−MMOB affinity of approximately 5 orders of magnitude (*27*, *30*).

The high-resolution X-ray crystal structure of MMOH and the NMR solution structure of MMOB have been reported for the components isolated from both *M. trichosporium* OB3b (*12*, *32*) and *Methylococcus capsulatus* (Bath) (*13*, *14*, *33*, *34*). Unfortunately, the MMOH−MMOB complex has never been crystallized, and thus, no structural data for the most active form of the enzyme are currently available. The X-ray crystal structures of MMOH reveal a "canyon" that exists between the two $\alpha\beta\gamma$ protomers that exposes the protein surface over the buried binuclear iron site. The dimensions of MMOB match those of the canyon, suggesting that it may exert its effects on the binuclear iron cluster by binding in this part of the MMOH structure, but no details of the surface interaction are known.

The NMR structure of MMOB shows that it has a well-ordered core (residues 36−126) flanked by N- and C-terminal regions that possess no significant structure in solution (residues 1−35 and 127−138). The N-terminus is known to contain residues essential for the overall MMOB function. In the case of *Me. capsulatus* (Bath) MMOB, N-terminal proteolysis and site-directed and deletion mutagenesis have been shown to reduce or eliminate the effects of the protein on catalysis (*35*, *36*). Similarly, we have observed that deletion of residues 2−29 of *M. trichosporium* OB3b MMOB does not affect the structure of the core region but does eliminate its ability to accelerate steady-state activity and the formation of **P** and **Q**.[2]

The structural fold of the core of MMOB does not suggest any obvious areas of MMOH−MMOB interaction, but the availability of the solution structure has made it possible to monitor changes in the environment of specific MMOB residues upon addition of MMOH. Perturbation of specific NMR resonances has been used to map interaction sites between MMOH and MMOB for both the *Me. capsulatus* (Bath) (*34*) and *M. trichosporium* OB3b systems.[2] In both cases, preliminary docking models have been constructed for the sites of interaction; however, there has been no direct study of the proposed contact sites.

In this study, through the combination of chemical modification, site-directed mutagenesis, and kinetics, we have located specific MMOB residues in both the N-terminal and core structural regions that play important roles in the MMO catalytic cycle. It is shown for the first time that MMOB

[2] More detailed structural studies are now in progress. S.-L. Chang, B. J. Wallar, J. D. Lipscomb, and K. H. Mayo, manuscript in preparation.

exerts regulatory influence throughout the catalytic cycle, and a potential new role for MMOB in substrate selection is revealed.

EXPERIMENTAL PROCEDURES

Reagents and Routine Procedures. Common reagents were the highest grade available and were obtained from either Sigma (St. Louis, MO) or Aldrich Chemicals (Milwaukee, WI). Molecular biological reagents were purchased from Qiagen, Inc. (Valencia, CA), Stratagene (La Jolla, CA), or Life Technologies, Inc. (Rockville, MD). DEAE-Sepharose and Sephadex resins were products of Pharmacia (Piscataway, NJ). Water was deionized and then further purified using a Millipore reverse osmosis system. Concentrations of the protein components and their respective activities were determined as previously described (*10*, *37*).

Bacterial Growth. For MMOH, the bacterial growth of *M. trichosporium* OB3b was as reported previously (*10*). For the isolation of MMOB, a recombinant MMOB system was used. The construction of the T7-based expression plasmid that contains the MMOB gene (*mmob*) has been reported previously (*32*). The plasmid yielded a high level of expression of *mmob* when subcloned into the BL21(SI) strain of *Escherichia coli* (Life Technologies, Inc.). BL21(SI) cells containing the mutant MMOB plasmids were cultured in LB broth (without NaCl) containing ampicillin (100 μg/mL) and grown at 32 °C in 2 L flasks with constant stirring and aeration. After reaching an OD of 0.8, cells were induced by the addition of NaCl to a final concentration of 300 mM. After growing for an additional 5 h at 30 °C, cells were harvested and centrifuged at 9000*g* for 20 min at 4 °C. The cell paste was subsequently stored at −80 °C. Typically, 3 g of cell paste/L of culture medium was obtained.

Site-Directed Mutagenesis of MMOB. Sequence analysis of MMOB was performed using the Wisconsin Package (version 8.1) by Genetics Computer Group (Madison, WI). The QuikChange system from Stratagene was used to construct the plasmids for all mutants of MMOB. All mutant *mmob* genes were sequenced by the University of Minnesota Microchemical Facility to confirm the constructs. The oligonucleotides used to introduce the mutations were H5A (5′-CATATGTCCAGCGCTGCGAACGCTTACAACGCC-3′ and 5′-GGCGTTGTAAGCGTTCGCAGCGCTGGACA-TATG-3′), H33A (5′-GGAGAACCAGGTCGTCGCCGAG-TCCAACGCCG-3′ and 5′-CGGCGTTGGACTCGGCGACG-ACCTGGTTCTCC-3′), and N107G/S109A/S110A/T111A (5′-CGACCTTCTCATCGGTGTGGCGGCGGCGGTCGG-CCGCGCC-3′ and 5′-GGCGCGGCCGACCGCCGCCGC-CACACCGATGAGAAGGTCG-3′).

Purification of Recombinant MMOB. All steps of the purification procedure were carried out at 4 °C. The cell paste (30−75 g) was suspended in 100 mL of 25 mM MOPS (pH 7.0). Cells were sonicated for 2 min with a total of three repetitions while maintaining the temperature at 4 °C with an ice bath, then diluted with an additional 350 mL of cold 25 mM MOPS (pH 7.0), and finally centrifuged at 25000*g* for 90 min. The supernatant was decanted and diluted with an additional 300 mL of 25 mM MOPS (pH 7.0). This cell free extract was loaded immediately onto a fast-flow DEAE Sepharose column (40 mm × 330 mm) equilibrated with 25 mM MOPS (pH 7.0) at a linear flow rate of 20 cm/h. The column was then washed with 1 L of 25 mM MOPS (pH 7.0) containing 0.08 M NaCl at a linear flow rate of 10 cm/h. The MMOB was eluted with a 1.6 L (800 × 800 mL) gradient from 0.08 to 0.25 M NaCl in the same buffer at a linear flow rate of 2 cm/h. Fractions were assayed for MMOB as previously described (*10*) and then pooled together. Solid $(NH_4)_2SO_4$ was added to the pooled MMOB fractions (50% of saturation) over the course of 30 min; the mixture was centrifuged at 9000*g* for 30 min, and then the precipitant was resuspended in a minimal amount of 25 mM MOPS (pH 7.0). This was loaded onto a Sephadex G-75 column (44 mm × 1000 mm) equilibrated in the same buffer, and the material was eluted at a linear flow rate of 1 cm/h. The pooled fractions containing MMOB activity were concentrated via ultrafiltration, frozen in liquid nitrogen, and stored at −80 °C.

Purification of MMOH. The purification of MMOH from *M. trichosporium* OB3b has been reported previously (*10*); however, a few modifications to this protocol have been made. The enzyme preparation was scaled up in cell weight by 3−5-fold (600−1000 g of cells). The size of the first DEAE-Sepharose Fast Flow column was increased to utilize 600 mL of resin, and the flow rate of the buffer used in ion exchange chromatography was increased by 5-fold. In this larger preparation of MMO, the pH of the hydroxylase fractions increased significantly to >8.0. Therefore, $^1/_{10}$ of the fraction volume of 500 mM MOPS (pH 7.0) was immediately added to each higher-pH fraction to neutralize MMOH. Purified MMOH exhibited specific activity in the range of 600−1200 nmol min^{-1} mg^{-1} for the turnover of furan.

Chemical Modification. Stock DEPC was first made by diluting 6.9 M DEPC (Sigma, St. Louis, MO) in cold ethanol to a concentration of 200 mM. The final modification reaction of MMOB by DEPC was as follows: 500 μM MMOB and 3.1 mM DEPC in 2.5 mL of 100 mM MOPS (pH 7.0). The reaction was allowed to proceed at room temperature with stirring and continuously followed spectrophotometrically at 244 nm. The reaction was finished in 10 min, after which imidazole was added to a final concentration of 50 mM to quench any potential nonspecific DEPC labeling. To a portion of this reaction mixture was added hydroxylamine to a final concentration of 100 mM and the mixture allowed to incubate at room temperature for 2 h. For the control (unlabeled) MMOB, all of the same conditions were used as in the labeling procedures; however, there was no DEPC present. For all reactions, after the appropriate reaction was complete, the entire sample was loaded onto a 10 mL Sephadex G-25 column and quickly eluted with 50 mM MOPS (pH 7.0). The fractions were assayed spectrophotometrically and pooled together. For the quantitation of modified histidines in the DEPC-treated MMOB, a difference spectrum centered at 244 nm was constructed by subtracting the control MMOB spectrum from the DEPC-labeled MMOB. Using an extinction coefficient of 3.2 mM^{-1} cm^{-1} for the modified histidine (*38*, *39*), a stoichiometry of 2.0 modified histidines/MMOB was calculated.

Steady-State Kinetic Measurements. For the multiple-turnover reactions with furan and methane, the reaction rates were monitored by measuring the rates of oxygen consumption using a Clark-type oxygen electrode fitted to a reaction chamber sealed with a very small bore (<0.5 mm) glass

stopcock to minimize the diffusion of air in and out of the reaction chamber. In all cases, the concentrations of the reaction components were as follows: 300 nM $MMOH_{act}$, 300 nM MMOR, and 0.4 mM NADH in 50 mM MOPS (pH 7.6). For furan turnover, 1.6 mM furan was present, and for methane reactions, 190 μM methane was used. The small amount of oxygen consumption that occurred in the absence of MMOB was always subtracted from the steady-state activity in the presence of MMOB. The amount of oxygen that was consumed was calibrated by quantitating the O_2 utilized during the turnover of 0.1 μmol of catechol by catechol 1,2-dioxygenase. Units of activity for furan and methane turnover are in turnover numbers per diiron site, and all experiments were performed at 25 °C.

For the multiple-turnover reactions with nitrobenzene, the reaction rates were monitored by the release of the product *p*-nitrophenol at 404 nm using an Agilent Technologies 8453 UV−vis spectrophotometer. In all cases, the concentrations of the reaction components were as follows: 1.0 μM $MMOH_{act}$, 1.0 μM MMOR, 1.2 mM nitrobenzene, and 0.4 mM NADH in 50 mM MOPS (pH 7.6). Using an extinction coefficient of 15 mM^{-1} cm^{-1} at pH 7.6 for *p*-nitrophenol, activity was then calculated in turnover numbers per diiron site. All of the nitrobenzene assays were performed at 25 °C.

Stopped-Flow Absorption Spectroscopy. The transient absorption measurements were all performed using an Applied Photophysics Ltd. SX.18MV stopped-flow spectrometer with the SK.1E extended spectrakinetic accessory (Surrey, United Kingdom). For single-turnover reactions, anaerobically reduced MMOH was made using the technique described by Fox et al. (*10*). In brief, MMOH and methyl viologen (0.1 mol/mol of MMOH) were made anaerobic in 50 mM MOPS (pH 7.0) in a 3 mL conical bottom reaction vial that was Teflon-sealed. The method of making the enzyme anaerobic was to simply flush the reaction vial with oxygen free argon gas for 30 min at 4 °C. Anaerobic sodium dithionite was then added stoichiometrically (1 mol of reducing equivalents/Fe or 2 mol of reducing equivalents/active site) to reduce the MMOH. The reaction was allowed to proceed on ice for about 30 min to ensure that the MMOH was fully reduced. For use in the stopped-flow spectrometer, the reduced MMOH was transferred to an anaerobic glass luer-lock syringe which was quickly attached to the stopped-flow sample delivery apparatus. The sample was then inserted into the drive syringe and allowed to incubate at the desired temperature for at least 10 min before data were collected.

For all experiments, O_2 was added in large excess over MMOH. Intermediates **P** and **Q** were monitored by following the 700 and 430 nm absorbance change, respectively, and all reactions took place at 4 °C. One syringe contained anaerobically reduced MMOH, and the other syringe contained the variable MMOB and substrate in O_2-saturated 50 mM MOPS (pH 7.0).

For the product release experiments, a high concentration of nitrobenzene was used (1.5 mM), and the reaction proceeded at 25 °C to allow the reaction of compound **Q** with nitrobenzene to occur very quickly. This facilitated observation of the product release step and comparison with the multiple-turnover reaction, which is rate-limited by this step. All product release experiments were monitored at 400 nm.

Transient Kinetic Data Analysis. Pseudo-first-order kinetics were generally observed because O_2 adds in an effectively irreversible step in the dead time of the stopped-flow instrument for all experiments, and the substrate concentrations are in excess over that of MMOH for most experiments. The reactions that were monitored usually consisted of at least two steps, each of which contributed a kinetic phase. The phases sum together to produce the overall time course. The number of relaxations that were observed defines the minimum number of steps in the reaction, but it does not define a specific mechanism or order for the steps. In the current case, rapid scan optical and time-resolved Mössbauer spectroscopies have shown that **P** forms prior to **Q** (*18*, *24*, *25*). If it is assumed that the steps are irreversible, then the relaxation times are equal to the reciprocal rate constants for the steps. Finally, amplitude analysis has been used to identify which relaxation time was associated with the formation of **Q** (*18*). The reciprocal relaxation times and amplitudes of the phases were determined by nonlinear regression fitting using the program KFIT developed by N. C. Millar of Kings College (London, England) as previously described (*18*). Rate constants listed in this paper were determined from analysis of at least 10 repetitions of each experiment.

Simulations of reaction time courses were completed using the numerical integration program KSIM version 2.0, also developed by N. C. Millar. This program allows a sequence of reactions to be entered along with reactant concentrations, rate constants for specific steps, and relative absorbance values of intermediates. The simulated time course can then be directly compared with the experimental data.

RESULTS

Kinetics of DEPC-Modified MMOB. The importance of the disordered N-terminal region of MMOB to efficient catalysis is apparent from the lack of activity of naturally truncated variants and deletion mutants (*35*, *36*).[2] The only histidine residues of the protein are found in this N-terminal region at positions 5 and 33 of MMOB isolated from *M. trichosporium* OB3b (*40*), *Methylocystis* sp. strain M (*41*, *42*), and *Methylocystis* sp. strain WI 14 (*43*) (see Figure 1). His33 is also conserved in the equivalent position of MMOB from *Me. capsulatus* (Bath) (*44*), although the equivalent of His5 is a Ser. Due to the lack of apparent secondary structure in this region, it seemed likely that the two His residues of MMOB could be easily and specifically modified by DEPC. DEPC was reacted with *M. trichosporium* OB3b MMOB as described in Experimental Procedures, resulting in the formation of 2.0 ethoxyformylhistidyl groups as shown by the characteristic absorbance at 244 nm. There was no evidence of additional incorporation at residues other than His.[3] Thus, it seems likely that the two His residues were specifically modified.

[3] Even though much less efficient, DEPC can also modify the nucleophilic side chains of other amino acids, including tyrosine, lysine, and cysteine. Upon addition of hydroxylamine at pH 7.0, the effect of DEPC was nearly completely reversed, indicating that cysteine or lysine was not modified to an appreciable extent. In the case of tyrosine, a significant modification would result in a change in the absorbance spectrum near 278 nm; however, no change was observed in the UV spectrum except near 244 nm which is expected for ethoxyformylation of histidine.

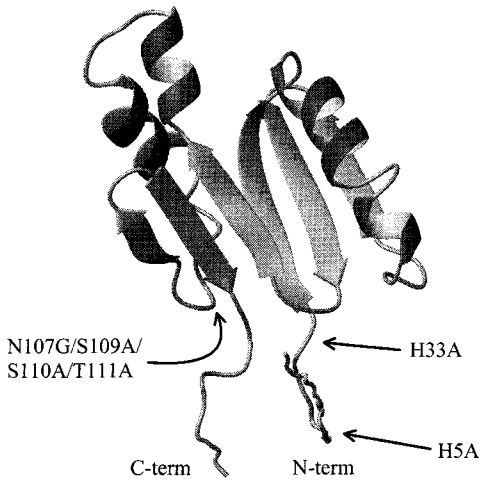


```
                10         20         30
B-OB3b   MSSAHNAYNAGIMQKTGKAFADEFFAEENQVVHESN
B-Bath   MSVNSNAYDAGIMGLKGKDFADQFFADENQVVHESD
B-strM   MSSAHNAYNAGIMQKTGKAFACEFFAEENQVVHESN
B-strWI  MTSAHNAYNAGIMQKTGKAFADEFFAEEXQVVHESN
T4MOD    MST                        LADQALHNNN
T3MO     MSI                        DNTAEAYRNN
TbmC     MSQ
PH3      MTS
P2       MSS

          40         50         60         70
B-OB3b   AVVLVLMKSDEIDAIIEDIVLKG GKAKNPSIVVED
B-Bath   TVVLVLKKSDEINTFIEEILLTDYKKNVNPTVNVED
B-strM   AVVLVLMKSDEIDAIIEEMVLKG GKAKNPSIVVED
B-strWI  AVVLVLMKSDEIDAIIEDIVLKG XKAKNPSIVVED
T4MOD     VGPIIRAGDLVEPVIETAEIDNPGKE     ITVED
T3MO     RVGPVLRASSITAGVIEAAQEDNPGKS     IRIDD
TbmC      VFIAFQANEESRAVIEAIVTDNPE       AVVTY
PH3      KVYLALQDNDTSRYIIEAIEQDNPE       ATIQY
P2       LVYIAFQDNDNARYVVEAIIQDNPH       AVVQH

                80         90         100
B-OB3b   KAGFWWIKADGAIEIDAAEAGELLGKPFSVYDLLIN
B-Bath   RAGYWWIKANGKIEVDCDEISELLGRQFNVYDFLVD
B-strM   KAGFWWIKADGAIEIDAAEAADLLGKPFSVYDLLVN
B-strWI  KAGFWWIKADGAIEIDAAEASDLLGKPFSVYDLLVN
T4MOD    RRAYVRIAAEGELILTRKTLEEQLGRPFNMQELEIN
T3MO     KLAYVRIDTDGELILRRATLEEALGRPFKMSELEVN
TbmC     PTGLVKIDAPGRLTIRRETIEEQTGRPFDLQQLHVN
PH3      LPAMIRVESTGELVVRAETVSEKLGQNWDIQELQLN
P2       HPAMIRIEAEKRLEIRRETVEENLGRAWDVQEMLVD

         110        120        130        140
B-OB3b   VSSTVGRAYTLGTKFTITSELMGLDRALTDI
B-Bath   VSSTIGRAYTLGNKFTITSELMGLDRKLEDYHA
B-strM   VSSTVGRAYTLGTKFTITSELMGLDRALTDI
B-strWI  VSSTVGRAYTLGTKFTITSELMGLDRALTDI
T4MOD    LASFAGQIQADEDQIRFY      FDKTM
T3MO     LSSFAGRIETTDDYVRFY      YEKTL
TbmC     LVTLSGHIDEDDDQLTLS      WQH
PH3      MITLGGNVDEDDDSFTLK      WN
P2       VITIGGNVDEDDDRFVLE      WKN
```

FIGURE 1: Protein sequence comparisons of MMOB with other non-heme oxygenase effector proteins. The protein sequences labeled are as follows: MMOB from *M. trichosporium* OB3b (B-OB3b), MMOB from *Me. capsulatus* (Bath) (B-Bath), MMOB from *Methylocystis* sp. strain M (B-strM), MMOB from *Methylocystis* sp. strain WI 14 (B-strWI), component D of toluene 4-monooxygenase from *Pseudomonas mendocina* (T4MOD), the effector protein of toluene 3-monooxygenase from *Pseudomonas picketti* (T3MO), the effector protein of toluene 2-monooxygenase from *Pseudomonas* sp. CF600 (Tbmc), the effector protein of phenol hydroxylase from *Acinetobacter calcoaceticus* (PH3), and the P2 effector protein of phenol hydroxylase from *Pseudomonas putida* (P2). The sequences in bold are identical residues in the four MMOB genes. Sequences were aligned using the Wisconsin Package (version 8.1) by Genetics Computer Group. The N-terminus of the MMOB structure that is shown has been truncated for the sake of clarity. Consequently, the position of H5 shown only indicates the general region of the structure in which it is located.

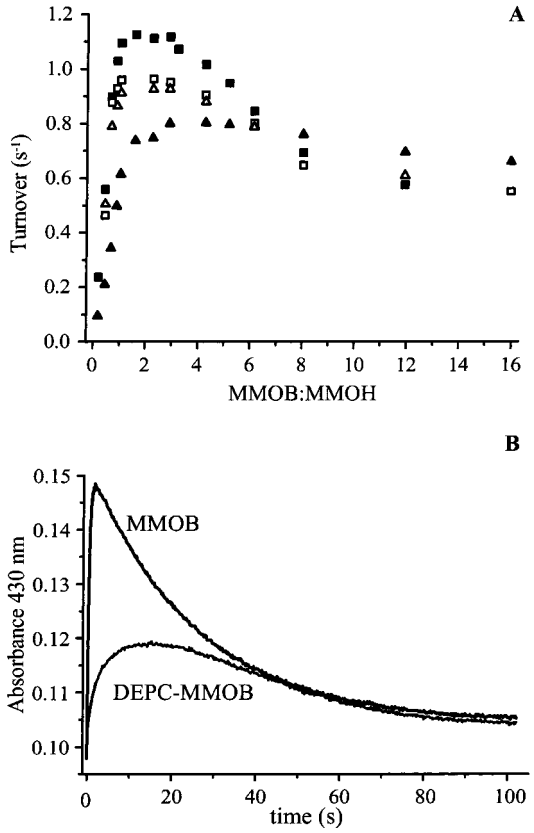

FIGURE 2: Steady-state kinetics of MMO turnover (A) and transient kinetics of MMOH single turnover (B) in the presence of DEPC-labeled MMOB or wild type MMOB. (A) Multiple turnovers of MMO using furan as the substrate. The assays were performed as described in Experimental Procedures. Units of activity are expressed in turnover numbers per diiron site. The different reactions are denoted as follows: wild type MMOB (■), DEPC−MMOB (▲), wild type MMOB + hydroxylamine (□), and DEPC−MMOB + hydroxylamine (△). (B) The time course of compound **Q** was followed at 430 nm via single-wavelength stopped-flow spectroscopy at 4 °C. The final reaction mixture included 25 μM $MMOH_{act}$, DEPC−MMOB, or wild type MMOB in 50 mM MOPS (pH 7.0). The appropriate fits are overlaid on the data. When the reaction was repeated a concentration that was 4 or 8 times the concentration of the DEPC−MMOB complex, a time course that can be superimposed with that shown was observed, suggesting that the complex between the DEPC−MMOB complex and MMOH is fully formed even when the components are present in a 1:1 ratio.

As shown in Figure 2A, the DEPC−MMOB complex was found to be 66% as active as control MMOB at an MMOB:MMOH stoichiometry of 2 using furan as the substrate.[4] The modified MMOB also appeared to have less of the characteristic inhibitory effect at high MMOB:MMOH ratios [due to the formation of additional component complexes which are unreactive in the case of unmodified MMOB (*27*)]. Upon addition of hydroxylamine, which specifically reverses the DEPC histidine modification, the steady-state activity in-

[4] MMOB alone does not actually possess an enzymatic activity; rather, it acts to enhance the catalytic turnover of substrates by the hydroxylase component of MMO. By maintaining the concentration of MMOH, MMOR, NADH, and substrate in steady-state assays, we found that measuring the degree of the MMOH activity enhancement as an indicator of MMOB function was valid. Therefore, even though MMOB does not catalyze the chemistry on the substrate, this paper refers to MMOB "activity" as the magnitude of the augmentation of MMOH activity.

creased to the equivalent of hydroxylamine-treated control MMOB.

The ability of the DEPC−MMOB complex to promote the formation of critical intermediate compound **Q** was also found to be altered as shown in Figure 2B. In accord with previous studies, the control MMOB time course monitored at 430 nm was fit to a summed two-exponential equation,[5] giving a **Q** formation rate constant of 2.70 s^{-1} and a decay rate constant of 0.039 s^{-1}. The DEPC−MMOB time course was markedly different, requiring three summed exponentials to achieve a good fit with **Q** formation rate constants of 0.77 s^{-1} (∼15% of the total amplitude) and 0.066 s^{-1} (∼85% of the total amplitude) and a **Q** decay rate constant of 0.039 s^{-1}. Thus, the modification of these two His residues specifically affects the formation but not the decay rate constant of **Q** in the absence of substrate.

Steady-State Activity of MMOB Histidine Mutants. To further explore the role of the MMOB histidines in multiple turnovers and the production of **Q**, three site-directed mutants were constructed: H5A, H33A, and H5A/H33A. Each mutant protein was overexpressed and purified in high yield as described in Experimental Procedures. One-dimensional NMR spectra of the mutant MMOBs were indistinguishable from those of the wild type and recombinant protein except for the position of modification, suggesting that no major structural changes occurred.[2] Steady-state kinetic analysis of the mutant MMOBs with furan (Figure 3A) or nitrobenzene (Figure 3B) as the substrate showed rather small changes in activity due to the modifications. The maximum activity of the H5A mutant was not significantly different than that of the wild type for both furan and nitrobenzene turnover. When furan was used as a substrate, H5A/H33A and H33A both had slightly lower activities at an MMOB:MMOH ratio of 2 compared to wild type (76 and 84%, respectively). No similar decrease in activity was observed when nitrobenzene was used as the substrate, although H5A/H33A did shift the point of optimal activity to a higher MMOB:MMOH ratio. The H5A/H33A double mutant also showed essentially no inhibitory effect for furan turnover at high MMOB:MMOH ratios, reminiscent of the effect of the DEPC−MMOB complex (Figure 2A). However, the inhibitory effect at higher MMOB:MMOH ratios was present in the H5A/H33A reactions with nitrobenzene. The apparent discrepancy between these observations can be explained by the method of detection of activity in the assays. For the furan assays, the reaction is monitored by the consumption of oxygen; therefore, it is possible that high relative concentrations of the mutated form of MMOB cause the enzyme to become partially uncoupled, resulting in a higher rate of utilization of O_2 than product formation. Indeed, adding a small aliquot of catalase to the completed H5A/H33A reaction mixture resulted in O_2 evolution, showing that a small amount of peroxide had been formed during the assay, which is not normally the case (data not shown). On the other hand, the nitrobenzene reaction is assayed by observing the release of product, so any uncoupling would not appear as an increase in activity as in the furan assay.

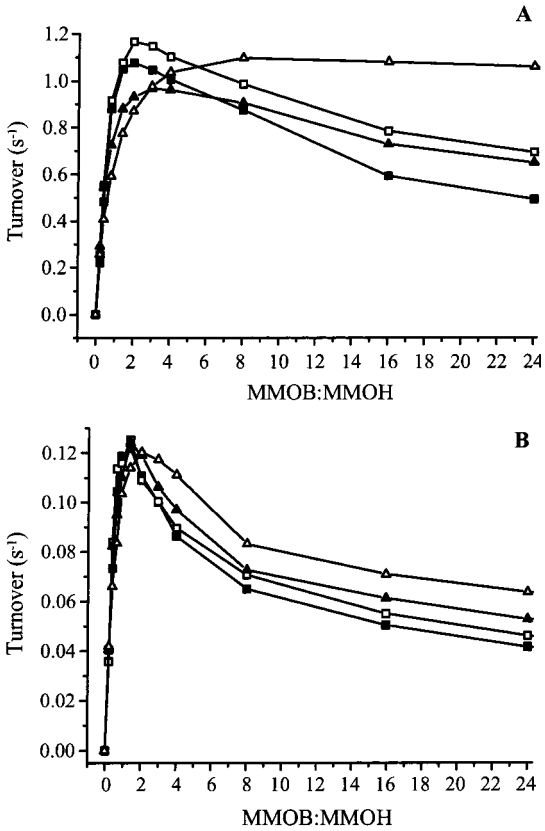

FIGURE 3: Steady-state activity of wild type MMOB and histidine mutants using furan (A) and nitrobenzene (B) as substrates. Both enzyme assays are described in Experimental Procedures. In both assays (A and B), the MMOB present was wild type (■), H5A (□), H33A (▲), and H5A/H33A (△). The data points for each MMOB are connected by line segments for clarity, but the presence of these lines does not indicate that they are fit to a specific model.

Steady-State Activity of N107G/S109A/S110A/T111A MMOB. Using the recently determined solution structures of MMOB from *M. trichosporium* OB3b (*32*) and *Me. capsulatus* (Bath) (*34*) and NMR techniques that detect MMOB residues that interact with MMOH, likely contact sites have been mapped (*34*).[2] The possible interaction area between MMOB residues 107 and 111 has substantial sequence homology between the two methanotrophs, as shown in Figure 1. As a result, the N107G/S109A/S110A/T111A MMOB mutant was constructed and shown by one-dimensional NMR studies to be structurally similar to wild type MMOB.[2] In steady-state activity studies of this quadruple mutant (Figure 4A), it was observed that for both furan and nitrobenzene, N107G/S109A/S110A/T111A MMOB had almost double the activity of wild type MMOB (1.8-fold for both substrates at peak MMOB:MMOH ratios). Nevertheless, the activity of N107G/S109A/S110A/T111A MMOB for methane turnover was not different from that of wild type MMOB as shown in Figure 4B.

*Compound **Q** Time Course with MMOB Mutants*. The fact that all of the mutant MMOBs yield active MMO systems and maximize the steady-state rate at approximately equimolar concentrations with MMOH suggests that they bind tightly to MMOH (see below) and promote the formation of the critical intermediate **Q**. The effect of each of the

[5] The fit to the time course of formation and decay of **Q** monitored at 430 nm actually requires at least three exponential phases (*45*). However, by far the greatest amplitude changes occur in the final two phases of the process which are slow relative to the kinetically isolated rapid phase that has a reciprocal relaxation time correlated with the **O**-to-**P*** step in the reaction cycle. Consequently, a two-exponential fit simplifies the data analysis and gives a reasonably good representation of the **P**-to-**Q** and **Q**-to-**T** steps of the reaction cycle.

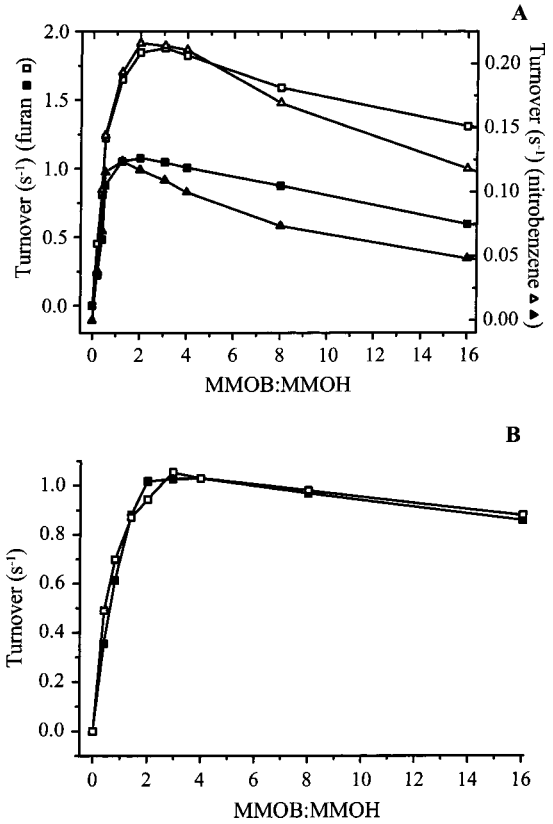

FIGURE 4: Steady-state MMO turnover in the presence of wild type MMOB or the N107G/S109A/S110A/T111A mutant using furan or nitrobenzene (A) or methane (B) as the substrate. The assays are described in Experimental Procedures. In the furan and nitrobenzene assays (A), the reaction mixture included wild type MMOB and furan (■), wild type MMOB and nitrobenzene (▲), N107G/S109A/S110A/T111A MMOB and furan (□), and N107G/S109A/S110A/T111A MMOB and nitrobenzene (△). The data points for each MMOB are connected by line segments for clarity, but the presence of these lines does not indicate that they are fit to a specific model. (B) For the methane assays, the reaction mixtures included wild type MMOB (■) or N107G/S109A/S110A/T111A MMOB (□).

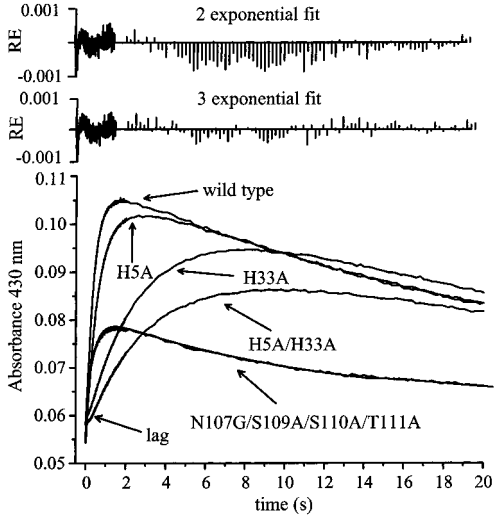

FIGURE 5: Single-turnover time course of **Q** formation and decay with wild type vs mutant MMOBs. **Q** was monitored at 430 nm over 102 s by using stopped-flow absorption spectroscopy (single-wavelength detector) and plotted over the course of 20 s. All time courses reached an equivalent final OD after the 102 s reaction. In each case, the final reaction mixture included 15 μM $MMOH_{act}$ and 15 μM MMOB in 50 mM MOPS (pH 7.0) at 4 °C. The data were fit to a summed two-exponential process with the rates given in Table 1. An example of a summed three-exponential fit of the **Q** time course with N107G/S109A/S110A/T111A MMOB is shown as a solid line superimposed on the data with the corresponding residual errors (RE) for two- and three-exponential fits displayed above. Fit parameters at 430 nm: $k_1 = 2.45\ s^{-1}$, $Amp_1 = 0.020$; $k_2 = 0.12\ s^{-1}$, $Amp_2 = -0.010$; $k_3 = 0.045\ s^{-1}$, $Amp_3 = -0.0084$.

Table 1: Rate Constants for Intermediates in a Single Turnover of $\mathbf{H}^r$ and O_2 at 4 °C[a]

MMOB	compound **P**[b] k_{form} (s^{-1})	compound **Q**[c] k_{form} (s^{-1})	compound **Q**[c] k_{decay} (s^{-1})
wild type	10.1 ± 1.1	2.70 ± 0.25	0.039 ± 0.003
H5A	9.4 ± 1.8	1.71 ± 0.20	0.036 ± 0.003
H33A	<0.35 ± 0.04[d]	~2.70[d]	0.036 ± 0.002
H5A/H33A	<0.28 ± 0.05[d]	~2.70[d]	0.034 ± 0.004
N107G/S109A/S110A/T111A	9.6 ± 1.0	2.45 ± 0.30	0.12 ± 0.001,[e] 0.045 ± 0.005

[a] General reaction conditions are given in Experimental Procedures. The temperature for all measurements was 4 °C. A single-wavelength detector was used for all measurements. The values that are shown are for fits to the data recorded at 430 nm except where noted. The values from fits to data recorded at 700 nm were the same within experimental error except where noted. Rate constants were determined from analysis of at least 10 repetitions of each experiment. [b] Since the **P** decay rate is the same as the **Q** formation rate, only the formation of **P** has been listed for clarity. This rate could not be directly determined from data monitored at 430 nm. The values shown are from fits to data recorded at 700 nm. The **P** formation rate was insensitive to substrate concentration. [c] The rate constants given for **Q** decay were measured in the absence of substrate. For **Q** decay rates in the presence of methane or furan, see Figure 6 and Table 2. In all cases, the **Q** formation rate was insensitive to substrate concentration. [d] Determination of these rate constants is discussed in further detail in the Results. [e] For the case of **Q** decay in the absence of substrate with N107G/S109A/S110A/T111A MMOB present, two decay rates were necessary to fit the data. The rate constant of 0.12 s^{-1} was responsible for about 60% of the decay, whereas 40% of the decay occurred at 0.045 s^{-1}. The reason for the split in the decay process is unclear. The presence of substrates eliminates the split decay.

mutant MMOBs on the time course of **Q** formation and decay in the absence of substrate is shown in Figure 5. For each of the histidine mutants, the **Q** time course was fit well by a summed two-exponential equation.[5] This indicates that the reaction consists of at least two steps as we have described in detail in previous studies (*18*, *20*). To the extent that the steps are irreversible, the reciprocal relaxation times of the exponential phases give the rate constants for the steps. The most significant effect on the **Q** time course was seen with the H33A and H5A/H33A mutants. While neither altered the decay rate constant of **Q**, they decreased the apparent (see below) formation rate constant significantly from 2.7 to 0.35 and 0.28 s^{-1}, respectively (see Table 1). The fact that the H5A/H33A mutant elicited only a slightly lower **Q** formation rate constant than H33A demonstrates that the major decrease in rate constant stems primarily from the histidine that is conserved in all methanotrophs studied in detail thus far, His33. The H5A mutation had a comparatively minor effect on the **Q** time course; however, it did consistently decrease the **Q** formation rate constant from 2.7 to 1.7 s^{-1}, again without changing the **Q** decay rate constant. We have observed in previous chemical modification studies of MMOB that some changes result in loss of activity due to the inability to form an MMOH−MMOB complex (*27*). Thus, it was conceivable that the change in rate constants observed here was due to incomplete complex formation,

resulting in non-first-order conditions and, consequently, irrelevant fits. However, superimposable time courses were observed for 4- and 8-fold excesses of the mutated MMOBs over MMOH active sites (data not shown). This demonstrates that a stoichiometric protein−protein complex forms in the dead time of the stopped-flow instrument and validates the initial proposal described above that the mutant MMOBs retain high affinity for MMOH.

The time course of **Q** formation and decay for the N107G/S109A/S110A/T111A quadruple mutant was quite different from the time courses of those forms of MMOB examined thus far in that **Q** reached a much lower maximum concentration. Fits to the time course (Figure 5) showed that three summed exponentials were required. **Q** was formed with a rate constant of 2.45 s^{-1}; however, the decay process apparently occurred in two steps. One step occurred with a rate constant of 0.12 s^{-1} (60% of the decay amplitude), while the second step exhibited a rate constant of 0.045 s^{-1}. The first step is 3-fold faster than observed using wild type MMOB, accounting in part[6] for the slower accumulation of **Q** (and also the decrease in the time at which the maximum accumulation of **Q** occurs as shown in Figure 5).

*Effect of Substrates on the Compound **Q** Time Course with MMOB Mutants.* The effects of the MMOB mutants on **Q** formation and decay in the presence of the substrates methane and furan were also examined (see Figure 6). In each case, the **Q** formation and decay time course could be fit by a summed two-exponential equation. The **Q** formation rate constant elicited by each mutant MMOB was unaffected by the presence of substrate. For both substrates with each of the mutants, the **Q** decay rate constant appeared to increase in a linear fashion with substrate concentration; thus, an apparent second-order rate constant for the process could be calculated from the slope of each plot (see Table 2).[7] In the case of methane, H5A and H33A elicited slightly smaller rate constants for **Q** decay, 7.2 ± 1.5 and 7.5 ± 1.0 mM^{-1} s^{-1}, respectively, compared to that of wild type MMOB (10.0 ± 1.1 mM^{-1} s^{-1}). In contrast, the N107G/S109A/S110A/T111A mutant caused a large decrease in the **Q** decay second-order rate constant, 1.4 ± 0.1 mM^{-1} s^{-1}.

When the larger substrate furan was used, wild type MMOB produced a second-order rate constant of 16 ± 2 mM^{-1} s^{-1} for **Q** decay. H5A and H33A again elicited slightly lower **Q** decay rate constants of 14 ± 1.5 and 12 ± 1.5 mM^{-1} s^{-1}, respectively. In contrast to the case described above for methane turnover, the quadruple mutant caused a large increase in the rate constant of the **Q** decay reaction with furan, 46 ± 5 mM^{-1} s^{-1}. This value is almost 3-fold higher than the second-order rate constant elicited by wild type MMOB. Thus, the interaction between the N107G/S109A/S110A/T111A quadruple mutant and MMOH causes large changes in both steady-state turnover and **Q** decay rate constants that are dramatically different for methane and a larger MMO substrate.

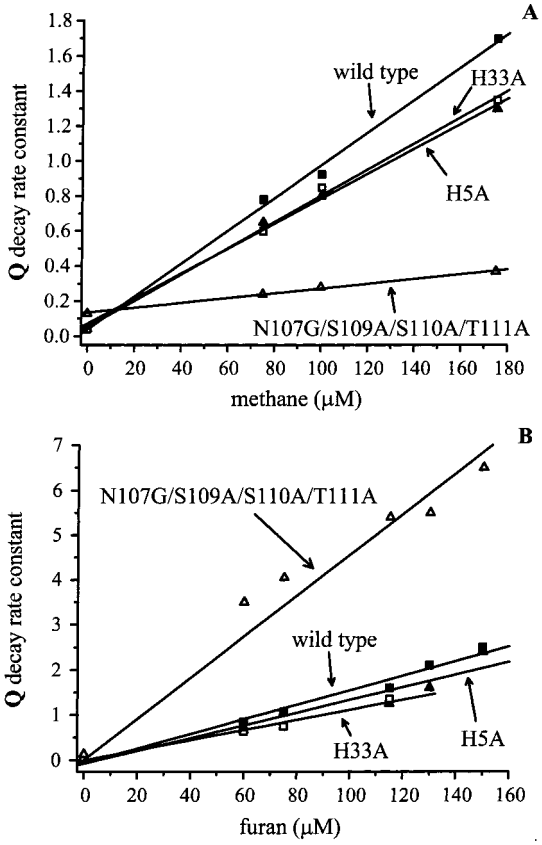

FIGURE 6: Dependence of the decay rate of **Q** on the concentration of the substrate methane (A) or furan (B) in the presence of wild type or mutant MMOBs. **Q** was monitored at 430 nm by using single-wavelength stopped-flow absorption spectroscopy. In each case, the final reaction mixture included 15 μM $MMOH_{act}$, 30 μM MMOB, and variable amounts of substrate in 50 mM MOPS (pH 7.0) at 4 °C: wild type MMOB (■), H5A (▲), H33A (□), and N107G/S109A/S110A/T111A (△).

Table 2: Second-Order Rate Constants for **Q** Decay in the Presence of Substrates and Wild Type MMOB or MMOB Mutants[a]

	k (mM^{-1} s^{-1})			
substrate	wild type MMOB	H5A	H33A	N107G/S109A/S110A/T111A
methane	10.0 ± 1.1	7.2 ± 1.5	7.5 ± 1.0	1.4 ± 0.1
furan	16.0 ± 2.0	14.0 ± 1.5	12.0 ± 1.5	46.1 ± 5.0

[a] Reaction conditions are given in Experimental Procedures. These values were obtained from experiments such as those shown in Figure 6. The pseudo-first-order rate constants that were used to calculate the second-order rate constants listed in this table were determined from analysis of at least 10 repetitions of each experiment.

*Effects on Compound **P** by MMOB Mutants*. Because **Q** formation and decay occurs at the end of an obligatory series of reactions beginning at $\mathbf{H^r}$, it is possible that the true effects of the mutated MMOBs may occur upstream of **Q** formation. Accordingly, the effects of these mutants on the kinetics of

[6] It is interesting to note that the maximum amplitude of the time course elicited by this mutant is consistently lower than would be expected on the basis of the rate constants relative to those observed for wild type MMOB. This is unlikely to be due to less formation of **Q** because observation of the time course at 700 nm shows that the same amount of **P** is formed, and the studies shown below in Figure 8 indicate that the same amount of product is formed when nitrobenzene is oxidized to nitrophenol. It is possible that **Q** formed in the presence of the quadruple mutant has a lower extinction coefficient than normal, potentially due to an effect such as greater solvent accessibility of the active site (see the Discussion).

[7] Our recent study suggests that the **Q** decay reaction is actually more complex than a one-step collisional process (*45*). The observation that temperature dependence studies of **Q** decay with methane yielded nonlinear Arrhenius plots, combined with the lack of an isotope effect for all MMO substrates other than methane, led to the proposal of a two-step process for **Q** decay. Nevertheless, the method in which the second-order rate constants were calculated in this study is a convenient technique for comparing **Q** decay reactions between mutants, as well as relating our findings to previous work.

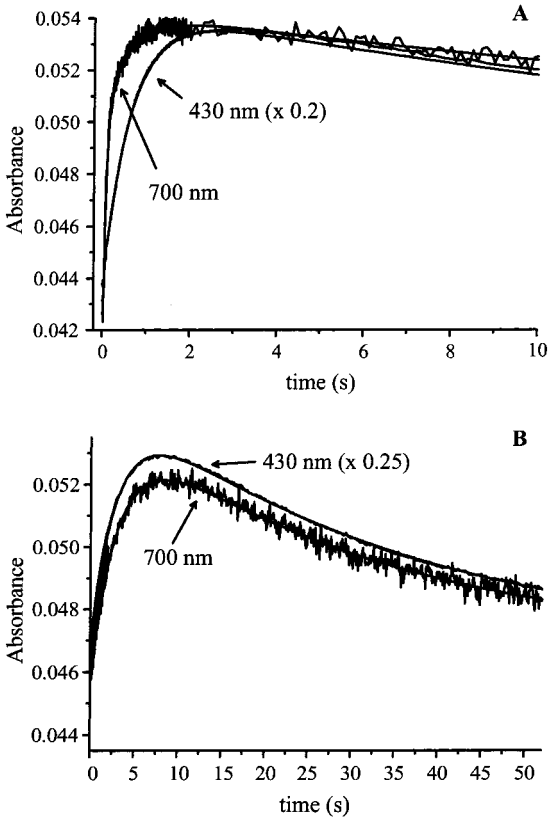

FIGURE 7: Time course of **Q** formation and decay monitored at 430 and 700 nm using H5A MMOB (A) or H33A MMOB (B). In each case, the final reaction mixture included 25 μM $MMOH_{act}$ and 25 μM MMOB in 50 mM MOPS (pH 7.0) at 4 °C. In both panels, the 430 nm data have been scaled down to clearly compare the trace to the 700 nm data. Panel A illustrates the initial 10 s of the reaction so that the relatively fast rate of formation of **P** can be clearly observed; however, the associated overlaid fit utilized all 100 s of data. Fits are shown as solid lines overlaying the data.

compound **P** formation were investigated. **P** was monitored by stopped-flow spectroscopy at 700 nm where it has a large extinction coefficient compared with the other intermediates in the catalytic cycle (*19*, *23*, *46*). For the cases of wild type MMOB, H5A, and the N107G/S109A/S110A/T111A quadruple mutant, the time course at 700 nm was fit to three summed exponential phases (an example is shown in Figure 7A). The reciprocal relaxation times of the first two phases give the rate constants of the formation and decay reactions of **P**, while the last phase yields the rate constant of the decay of **Q**, which also absorbs at 700 nm, albeit much more weakly than at 430 nm. The rate constants for **P** formation are listed in Table 1. The decay rate constant of **P** and the decay rate constant of **Q** were found to be the same within the uncertainty of the measurements as the formation and decay rate constants of **Q**, respectively, determined using the 430 nm data that are listed in Table 1. The wild type MMOB yielded a **P** formation rate constant of 10.1 ± 1.1 s^{-1}, while the H5A and N107G/S109A/S110A/T111A mutants gave similar **P** formation rate constants of 9.4 ± 1.8 and 9.6 ± 1.0 s^{-1}, respectively. Therefore, the slower rate constant of **Q** formation elicited by H5A (1.7 vs 2.7 s^{-1} for the wild type) cannot be due to a slower process prior to the step in which **Q** is formed.

Unexpectedly, the 700 nm time courses of **Q** formation and decay elicited by the other two His mutants, H33A and H5A/H33A, required only two summed exponentials to fit

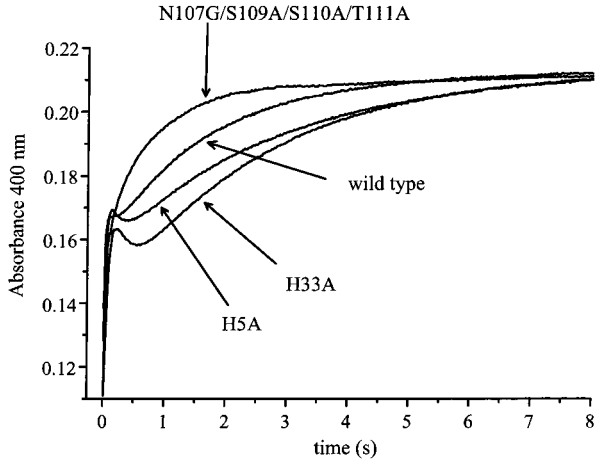

FIGURE 8: Time course of the single-turnover reaction of nitrobenzene with $\mathbf{H}^{\mathbf{r}}$ in the presence of wild type and mutant MMOBs. The reaction was followed by stopped-flow spectroscopy at 400 nm to optimize detection of the product *p*-nitrophenol. The final reaction mixture contained 25 μM $MMOH_{act}$, 25 μM MMOB, and 1.5 mM nitrobenzene in 50 mM MOPS (pH 7.6) at 25 °C.

the data (see an example in Figure 7B). This analysis yielded the same rate constants as were derived from 430 nm data (Table 1) of the same reactions where **P** cannot be observed due to the large absorbance of **Q**. Thus, it appears that **Q** formation and decay were being monitored at 700 nm and **P** formation is not observed for these mutants.

To illustrate the effects of the mutant MMOBs, Figure 7 also shows a comparison of the $\mathbf{H}^{\mathbf{r}}$ single-turnover reactions monitored at 430 or 700 nm. In both panels, the trace of the reaction monitored at 430 nm has been scaled down appropriately so that it visually overlays with the 700 nm trace. For H5A (Figure 7A), the fit to the 700 nm data required a fast exponential phase to accommodate the initial rapid **P** formation reaction. However, when using H33A (Figure 7B), both the 430 and 700 nm time courses lack the initial fast phase and are fit with the same summed two exponentials differing only in amplitudes. The ratio of the amplitudes at the two wavelengths is the same as the known ratio of the extinction coefficients of **Q** at these two wavelengths, supporting the proposal that only **Q** is observed in each case. Failure to observe **P** at 700 nm suggests that its rate of formation is greatly decreased so that none builds up during the reaction. This is confirmed by numerical integration simulations of the reactions showing that an at least 50-fold decrease in the **P** formation rate is required to account for the data (simulation not shown). Thus, the probable cause of the great decrease in the observed rate constant for **Q** formation when using H33A MMOB is the decreased concentration of the precursor **P**.

Effects on Product Release by Mutant MMOBs. The product of the MMO-catalyzed oxidation of nitrobenzene, *p*-nitrophenol, absorbs strongly at 404 nm, but only after it is released from the MMOH active site. Consequently, the decay rate constant of compound **T**, the product complex, can be easily determined (*18*). Shown in Figure 8 are the time courses of the formation and release of *p*-nitrophenol for the reactions employing wild type MMOB and three of the mutants. The reactions were allowed to proceed at 25 °C with a high substrate concentration so that the decay of **Q** would be much faster than the product release, and so that the results could be compared with the results of the

Table 3: Rate Constants for a Single Turnover of $\mathbf{H}^{r}$ in the Presence of 1.5 mM Nitrobenzene at 25 °C[a]

MMOB	compound **Q**		compound **T**
	k_{form} (s^{-1})	k_{decay} (s^{-1})	k_{decay} (s^{-1})[b]
wild type	56 ± 5	4.4 ± 1	0.63 ± 0.05
H5A	41 ± 5	4.0 ± 1	0.35 ± 0.05
H33A	14 ± 2	3.8 ± 1	0.42 ± 0.05
H5A/H33A	12 ± 2	4.0 ± 1	0.40 ± 0.05
N107G/S109A/S110A/T111A	59 ± 5	30 ± 2	1.30 ± 0.05

[a] The experiments were conducted as described in Experimental Procedures. The rate constants were determined by a combination of nonlinear regression fitting and numerical integration simulations as described in the text. [b] In addition to this decay process, a nonspecific process occurs at the end of the reaction that results in a small increase in the final OD of the product. The rate constant for this process was found to be quite variable, but was typically 0.005 s^{-1}. This means that it does not occur at a kinetically competent rate as part of the reaction cycle.

multiple-turnover experiments described above. The time courses were difficult to fit directly because it was found that at least four summed exponentials were required, and this is too many for a reliable fit by nonlinear regression procedures. Consequently, a fit was obtained by first estimating the **Q** formation and decay rates using data recorded at 550 nm where there is little contribution from **T** or *p*-nitrophenol. These values were then used as constants in nonlinear regression fitting procedures to estimate the rate constants for the **T** decay rate constants from data recorded at 400 nm. Finally, all of these values were used to begin trial and error fitting using numerical integration of the rate equations describing the complete **Q** formation and decay process, so the entire time course at 400 nm could be fit. Little change from the estimated values was required. This analysis suggests that the four observed steps are **Q** formation, **Q** decay, product release from **T**, and slow further increase in the absorbance of the product. The rate constants for the first three of these processes are shown in Table 3. The OD change for the final process was small, and the rate constant was at least 1 order of magnitude smaller than the turnover number for nitrobenzene; thus, this step is not kinetically competent and cannot be part of the reaction cycle. It may represent a change that *p*-nitrophenol undergoes in solution after its release.

At early times in the reaction elicited by wild type MMOB and H5A, the rapid formation and decay of **Q** to form **T** can be easily observed as a sharp rise and then a slight decrease in the time course. The decay of **Q** is seen as only a small decrease because **T**, which has *p*-nitrophenol bound, has a slightly lower extinction coefficient than **Q** at 400 nm. The absorbance then increases at longer times because the highly chromophoric product is released. The **Q** decay rate constants for wild type MMOB and the histidine mutants are all 4−5 s^{-1}. In the case of the H33A and H33A/H5A mutants, the formation of **Q** is slower as observed for the substrate free reaction at 4 °C described above, leading to a delay in the product release reaction, and thus, a slightly larger absorbance decrease is observed before product release dominates the absorbance change. The rate constant of product release is similar using the wild type MMOB or the histidine mutants, although the rates with the latter are slightly lower. Because product release is rate-limiting in the catalytic cycle, these values are consistent with the steady-state activity data (Figure 3) that showed similar rates of turnover for reactions with the histidine mutants and wild type MMOB at an MMOB:MMOH ratio of 2.

The absolute values for the turnover number shown in Figures 3 and 4 are slightly lower than the decay rate constants for **T** shown in Table 3. We have previously shown that this is due to the need to form a stoichiometric MMOH−MMOB−MMOR complex to optimize turnover (*27*). At the concentrations used for steady-state assays, this requires a several-fold excess of MMOR to make electron transfer non-rate-limiting. Such an excess was not used in the experiments shown in Figures 3 and 4. However, addition of excess MMOR resulted in approximately 3-fold increases in the maximum rate (data not shown), in accord with our previous studies (*27*).

The early portion of the reaction using the N107G/S109A/S110A/T111A quadruple mutant appears quite different because very little of the **Q** formation is observed and the plateau from formation of **T** is almost absent. This is consistent with the observation at 4 °C that the quadruple mutant greatly accelerates the **Q** decay reaction for large substrates (Figure 6). A good fit was obtained if the **Q** decay rate was assumed to be accelerated about 6-fold over that elicited by wild type MMOB, in reasonable agreement with the data depicted in Figure 6 (furan turnover at 4 °C). The release of product was also found to be accelerated by the quadruple mutant to about 2 times the rate elicited by wild type MMOB, probably accounting for the increased turnover number for nitrobenzene oxidation in the reaction mixture containing the quadruple mutant (Figure 4).

*Kinetics of **Q** Formation and Decay in the Presence of a Mixture of MMOB Mutants*. The results presented thus far show that the H33A mutant dramatically slows the **Q** formation process (probably at the **P** formation step), while the N107G/S109A/S110A/T111A quadruple mutant significantly slows the **Q** decay step during methane oxidation. There are many possible outcomes if both of these mutants are present simultaneously depending upon the rate of exchange of the MMOH−MMOB complex. For example, if the MMOBs exchange rapidly relative to the reactions of the cycle, it is possible that the mutant that induces the faster rate will dominate in each part of the reaction, so fast **Q** formation and decay will be seen. Alternatively, no exchange may occur, in which case the slow and fast reactions induced by each mutant will occur independently and some average of the fast and slow rates will be observed in the **Q** time course. Finally, MMOB exchange might occur rapidly in one part of the **Q** time course and slowly in the other to give yet another observed time course. Figure 9 shows the **Q** formation and decay time course in the presence of methane and a 1:1:1 mixture of H33A, quadruple mutant, and $MMOH_{act}$ along with simulations of the predicted time courses based on the rate constants reported above for the reactions elicited by the isolated mutants. The only simulation that matches the observed time course is that made under the assumption that MMOB does not exchange rapidly between the formation of **P** and the formation of **T**. The simulation was made under the assumption that the mutant forms bind to MMOH with equal affinity. The excellent fits that were obtained validate this assumption and support the

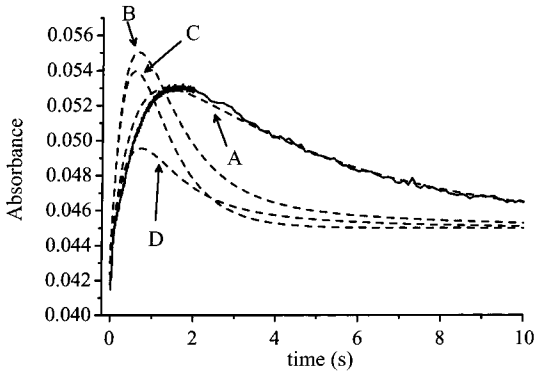

FIGURE 9: Time course and simulations of the single-turnover reaction of methane with $\mathbf{H^r}$ in the presence of a mixture of H33A and N107G/S109A/S110A/T111A mutant MMOBs. The reaction mixture contained 25 μM $MMOH_{act}$, 25 μM H33A, and 25 μM quadruple mutant in 50 mM MOPS (pH 7.0) at 4 °C containing 0.1 mM methane. The observed reaction time course (—) was simulated (— — —) using the following rate constants: H33A, apparent **Q** formation $k = 0.3\ s^{-1}$ and **Q** decay $k = 1\ s^{-1}$; quadruple mutant, **Q** formation $k = 2.4\ s^{-1}$ and **Q** decay $k = 0.2\ s^{-1}$. The simulation are for (A) formation of MMOH mutant MMOB complexes that do not exchange, (B) exchange up to the point of **Q** formation, but no exchange during product formation, (C) free exchange in all steps, and (D) no exchange up to **Q** formation but free exchange during product formation. All reaction steps in the simulations are assumed to be irreversible as appears to be the case for the actual reactions.

proposal made above that the mutations do not greatly affect the affinity of MMOB for MMOH.

DISCUSSION

MMOB is a member of a large group of "effector" proteins that are part of multicomponent oxygenase systems (*10*, *42*, *47*−*57*). These proteins are necessary for efficient catalysis and generally prevent competing processes that might lead to uncoupling, generation of diffusable reactive oxygen species, or the oxidation of adventitious substrates that cannot be further metabolized. Although the specific function of the effector protein differs from system to system, the mechanism of implementation always involves the formation of a complex with the active site-containing oxygenase component with attendant changes in its physical and/or kinetic properties. In no case to date has the structural interaction between the effector and the oxygenase been determined in sufficient detail to state how the observed changes in the catalytic properties of the oxygenase are brought about. Also, it has proven to be difficult to ascertain whether the effector continues to exert its influence on the oxygenase in steps of the catalytic cycle beyond the last relatively stable species which is amenable to spectroscopic and thermodynamic studies in each enzyme system.

In this study, we have begun to address these problems by using chemical modification and site specific mutagenesis to identify specific residues in both the disordered N-terminal region and the well-ordered core region of MMOB that perturb the kinetics of interconversion of the intermediates in the MMOH catalytic cycle. Through this and previous studies, modified MMOBs are now available that demonstrate for the first time that this effector exerts its influence throughout the MMO catalytic cycle. Knowledge of the MMOB residues that affect specific steps in MMOH catalysis gives insight into the mechanisms by which this effector protein functions which are discussed in the following sections.

N-Terminal Mutations. Previous studies of the N-terminal region of MMOB have focused on the fact that it can be cleaved by either endogenous proteases during preparation or by deletion mutagenesis (*35*, *36*).[2] It has been shown that the modification of specific residues in the N-terminal region can prevent or retard proteolysis, and that controlled N-terminal truncation can reduce and eventually eliminate the MMOB effects on catalysis. The focus of the current study is different in that the goal was to begin to determine the function of the N-terminus through modification or mutation of conserved residues. The histidine at position 33 is conserved in MMOB from all four methanotrophs listed in Figure 1, as well as component D of toluene 4-monooxygenase (T4MOD). In the MMOB structure, this residue is near the point where the flexible, ill-defined N-terminus joins the well-structured core of the protein. In the MMOBs from three of the methanotrophs, H33 is the sixth residue in a string of eight identical amino acids (ENQVVHES). His5 is conserved in three of the four MMOB sequences that are known, but this section of the protein is not present in other similar oxygenase effectors (Figure 1). Nevertheless, its presence near the N-terminus and the inhibitory effects of its chemical modification made it a good target for mutagenesis.

Neither mutant significantly affected the steady-state turnover number, but both conserved histidine residues were found to affect the rate of interconversion of reaction cycle intermediates. This is possible because product release is significantly rate-limiting, and thus, substantial rate changes can occur in earlier steps in the catalytic cycle without changing the turnover number. Interestingly, the two histidine mutants affect different steps in the catalytic cycle. His5 is apparently necessary for the maximum rate of O−O bond breaking to be realized during the conversion of intermediate **P** to **Q**. On the other hand, His33 appears to be required to efficiently form either **P** or an intermediate before **P**, i.e., either **O** or **P***. We know this is the case because there is no observed buildup of **P** when the reaction is monitored at 700 nm where **P** is readily observed. Our past studies have shown that if the MMOB−MMOH complex does not form, the rate of the $\mathbf{H^r}$ single turnover is decreased by 1000-fold by directly or indirectly preventing O_2 binding to the cluster to form **P*** (*20*). As a result, there is no observable buildup of **P** or **Q**, although it is likely the reaction still passes through these intermediates because methane is oxidized at a slow rate. In the case of H33A, it appears that a strong complex with MMOH is still formed based on the facts that (i) a normal MMOB concentration dependence is observed for steady-state turnover, (ii) the single-turnover reaction time course is affected up to, but not beyond, a 1:1 MMOB:MMOH stoichiometry, (iii) nearly normal amounts of **Q** build up during single-turnover reactions, and (iv) the affected reaction cycle step is only slowed by about 50- rather than 1000-fold. If it is assumed that this complex is formed, it seems likely that O_2 binding will occur and intermediates **O** and **P*** will be formed rapidly so that the decreased rate of **Q** formation elicited by H33A would be due to a slowing of the **P*** to **P** reaction. This hypothesis can best be examined by freeze-quench EPR and Mössbauer studies, which are in progress. However, some insight can be gained from careful

examination of the first 100 ms of the time course of the reaction monitored at 430 nm, which reveals a lag phase (marked in Figure 5) that we have previously shown to be due to the formation of weakly absorbing intermediates **O**, **P***, and **P** prior to **Q** (*45*). The duration and shape of this lag are dependent on the rate constants for intermediate conversion. Simulations of the H33A-elicited reaction time course by numerical integration show that the observed lag phase is matched most precisely when the slow step is introduced in the **P*** to **P** step.

The basis for the decrease in rate constant for formation of the **P** and **Q** intermediates by the H33A and H5A MMOB mutants, respectively, is unknown, but the fact that histidine residues are involved suggests an intriguing possibility. Our past work has shown that the rate constants for formation of both **P** and **Q** are pH-dependent. Moreover, solvent isotope effect studies have suggested that one proton is supplied in each step through a "one-hop" process from a group with a fractionation factor near 1 and a pK_a near neutral (*19*). One possibility for the source of these protons is solvent in the active site or bound to the cluster. The fact that mutations of the histidine residues specifically affect the two steps in which the protons are transferred suggests that they may play some role in this process. For example, they may facilitate the movement of protons from solution to the species in the active site that directly donates the protons for catalysis.

The effects of the histidine mutants on the rate constants of **P** and **Q** formation may also be purely structural. Past studies have shown that the iron−iron distance in the cluster must change dramatically at each step of the catalytic cycle to accommodate the new form of oxygen present in each (*12*, *13*, *24*, *58*). Any interaction with MMOB that facilitates the implied conformational change in the protein structure supporting the cluster will promote interconversion of the intermediates. Thus, disruption of the interaction could alter the interconversion rate.

The presence of alanine mutations at both positions 5 and 33 causes effects similar to those observed for the H33A mutation alone. This is expected because the effect on the rate constants is at least 30-fold greater for the H33A mutant than for the H5A mutant. Nevertheless, there is still a 20% decrease in the rate constant of **Q** formation in the double mutant over H33A alone, suggesting that there are additive effects. The uncoupling observed exclusively for the double mutant in multiple-turnover experiments using furan as a substrate cannot be definitively accounted for at present. Past studies have shown that in the absence of MMOB the overall product yield from a single-turnover reaction is ∼40%, which increases to 80% in the presence of MMOB and 100% when MMOB and MMOR are present (*20*). We postulated that the "leak" occurs at the step of **P** to **Q** conversion in the absence of MMOB. In the case of the H5A/H33A mutant MMOB, however, the yield of *p*-nitrophenol from nitrobenzene turnover is the same as when wild type MMOB is used in the reaction (based on data similar to those shown in Figure 8), so the single-turnover reaction remains highly coupled. It is possible that the double mutant perturbs the MMOR−MMOH complex so that autoxidation of MMOR occurs more readily during turnover.

MMOB Core Mutations. Although the core structure of MMOB alone is clearly not sufficient to allow MMOB to act as an effector[2] (*35*, *36*), the results of this study show that it can have a large effect on catalysis. Current work on the *M. trichosporium* OB3b $\mathbf{H^{ox}}$−MMOB interactions[8] suggests that electrostatic interactions play an important role in stabilizing the component complex. As a result, a loop of four polar residues (N107, S109, S110, and T111) that showed evidence for interaction with MMOH in NMR studies, and which are conserved in three of the four methanotroph MMOB sequences (Figure 1), was selected for mutagenesis. It should also be noted that N107 and S110 are homologous among all of the oxygenase effector proteins listed in Figure 1. All four polar residues were replaced with smaller nonpolar side chains to generate the quadruple mutant.

Although our expectation was that this mutation would inhibit catalysis, the opposite result was observed. No change was found for steady-state methane turnover, while the turnover number for large substrates was nearly doubled. It is significant that the absolute values for the turnover numbers for furan and nitrobenzene differ by about 10-fold, so the fact that both double in the presence of the quadruple mutant suggests that it is their bulk rather than their reactivity that is important. Examination of the kinetics of interconversion of reaction cycle intermediates showed that the steps in **Q** formation were not affected by this mutation, but all the steps following **Q** formation were altered. The rate constant for **Q** in the absence of substrates was increased 3-fold, as was the second-order rate constant for the reaction with furan. Remarkably, the second-order rate constant for the reaction with methane decreased substantially, clearly differentiating methane from larger substrates in the reaction with **Q**. Even at the slower rate, the **Q** decay in the presence of methane does not become rate-limiting overall, so it would not be expected to affect the turnover number, as observed. Accordingly, this observation supports the proposal that product release is rate-limiting for methanol, just as it is for *p*-nitrophenol.

The effects of the quadruple mutant cannot be rationalized in detail without further structural studies. However, the fact that its effects seem to depend on the size of the substrate allows some speculation. Recently, we have shown that the **Q** decay reaction occurs in at least two steps which are nominally described as substrate binding and C−H bond breaking (*45*). It is possible that a substrate also binds in the second step. Kinetic studies showed that CH_4 exhibits a deuterium isotope effect of 50−100 in the **Q** decay reaction, while C_2H_6 exhibits no isotope effect. One explanation for both of these observations, suggested by the completely enclosed active site of MMOH (*12*−*14*), is that the enzyme structure makes methane C−H bond breaking rate-limiting while larger substrates encounter a rate-limiting binding process. In effect, the enzyme acts as a molecular sieve sized for methane to enhance its turnover rate. On the basis of its effects in increasing the rate of the O_2 reaction with $\mathbf{H^r}$ and its effects on substrate reaction with **Q** demonstrated here, MMOB may be an important component in allowing molecules the size of O_2 and CH_4 preferred access to the diiron cluster. When the residues of the quadruple mutation are altered to smaller, less polar residues, larger substrate molecules may be admitted more easily by MMOB, increasing the rate of the reaction with **Q** as illustrated in Scheme

[8] B. J. Wallar and J. D. Lipscomb, manuscript in preparation.

Scheme 2: Hypothesis for the Interaction of N107G/S109A/S110A/T111A MMOB with the Active Site of MMOH[a]

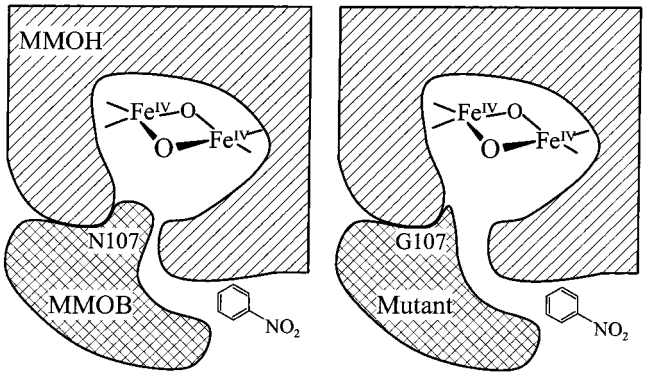

[a] A minor disruption in the MMOB-MMOH interactions at this loop region on MMOB may allow for increased access of larger substrates and products to enter and exit the active site.

2. Similarly, the larger substrates may depart from the active site more rapidly, increasing the turnover number. The departure of the small product methanol would not be expected to be affected by the quadruple mutant, in accord with our results; however, the large decrease in the reaction rate with methane with **Q** is difficult to understand. It is possible that the nearly completely hydrophobic active site of MMO effectively concentrates methane from solution, and this is compromised if greater access to solvent is permitted by the binding of the quadruple mutant.

Conclusion. The mutations examined here have relatively small effects on turnover number determined using steady-state kinetics, but they yield a great deal of information about the effects of MMOB on the intermediates of the catalytic cycle of MMOH. This underscores the value of using the single-turnover approach to critically examine the effects of mutagenesis on catalysis. Using this approach in this and previous studies, we have been able to show that (i) binding of MMOB is required for efficient reaction of $\mathbf{H}^{\mathbf{r}}$ with O_2 to form **P*** and perhaps also **O**, (ii) MMOB plays a role in the rapid formation of **P**, probably by strongly accelerating the step in which it is formed, (iii) MMOB also accelerates **Q** formation, (iv) both the autodecay and the substrate-induced decay of **Q** are affected strongly by MMOB in a manner that depends on the size of the substrate when present, and (v) the release of large substrates from **T** is accelerated by MMOB. Thus, we must now think about MMOB in the context of a regulator of each step in the catalytic cycle. This represents a large expansion in the role of MMOB and underscores its importance to catalysis. It also presents new opportunities to isolate and characterize the intermediates of this archetypal cycle of oxygen activation through fine control of the rates of progression from step to step. Finally, MMOB can now be considered to be a modular protein with at least two functional domains, namely, a well-folded core domain and a disordered N-terminal domain. The domains must both be present to observe function from either, but once this criterion is satisfied, the N-terminal domain seems to be directed toward regulation of the formation of **Q** while the core domain regulates its decay. Finally, by taking advantage of the fact that the H33A and quadruple mutants affect the rate constants of different steps in the cycle, it has been shown the MMOB does not exchange during the portion of the cycle when the reactive intermediates are made and utilized. This is the first insight into the dynamics of protein–protein interaction in MMO regulation and provides a framework for future studies of the remarkable ability of MMOB to control monooxygenase catalysis.

ACKNOWLEDGMENT

We thank Shou-Lin Chang and Kevin H. Mayo for measurement of NMR spectra and many useful discussions.

REFERENCES

1. Wallar, B. J., and Lipscomb, J. D. (1996) *Chem. Rev. 96*, 2625−2657.
2. Feig, A. L., and Lippard, S. J. (1994) *Chem. Rev. 94*, 759−805.
3. Lipscomb, J. D. (1994) *Annu. Rev. Microbiol. 48*, 371−399.
4. Dalton, H. (1980) *Adv. Appl. Microbiol. 26*, 71−87.
5. Takeguchi, M., Miyakawa, K., and Okura, I. (1998) *J. Mol. Catal. A: Chem. 132*, 145−153.
6. Nguyen, H. H., Elliott, S. J., Yip, J. H., and Chan, S. I. (1998) *J. Biol. Chem. 273*, 7957−7966.
7. Zahn, J. A., and DiSpirito, A. A. (1996) *J. Bacteriol. 178*, 1018−1029.
8. Semrau, J. D., Zolandz, D., Lidstrom, M. E., and Chan, S. I. (1995) *J. Inorg. Biochem. 58*, 235−244.
9. Stanley, S. H., Prior, S. D., Leak, D. J., and Dalton, H. (1983) *Biotechnol. Lett. 5*, 487−492.
10. Fox, B. G., Froland, W. A., Dege, J. E., and Lipscomb, J. D. (1989) *J. Biol. Chem. 264*, 10023−10033.
11. Fox, B. G., Surerus, K. K., Münck, E., and Lipscomb, J. D. (1988) *J. Biol. Chem. 263*, 10553−10556.
12. Elango, N., Radhakrishnan, R., Froland, W. A., Wallar, B. J., Earhart, C. A., Lipscomb, J. D., and Ohlendorf, D. H. (1997) *Protein Sci. 6*, 556−568.
13. Rosenzweig, A. C., Nordlund, P., Takahara, P. M., Frederick, C. A., and Lippard, S. J. (1995) *Chem. Biol. 2*, 409−418.
14. Rosenzweig, A. C., Frederick, C. A., Lippard, S. J., and Nordlund, P. (1993) *Nature 366*, 537−543.
15. Fox, B. G., Hendrich, M. P., Surerus, K. K., Andersson, K. K., Froland, W. A., Lipscomb, J. D., and Münck, E. (1993) *J. Am. Chem. Soc. 115*, 3688−3701.
16. DeWitt, J. G., Bentsen, J. G., Rosenzweig, A. C., Hedman, B., Green, J., Pilkington, S., Papaefthymiou, G. C., Dalton, H., Hodgson, K. O., and Lippard, S. J. (1991) *J. Am. Chem. Soc. 113*, 9219−9233.
17. DeWitt, J. G., Rosenzweig, A. C., Salifoglou, A., Hedman, B., Lippard, S. J., and Hodgson, K. O. (1995) *Inorg. Chem. 34*, 2505−2515.
18. Lee, S.-K., Nesheim, J. C., and Lipscomb, J. D. (1993) *J. Biol. Chem. 268*, 21569−21577.
19. Lee, S. K., and Lipscomb, J. D. (1999) *Biochemistry 38*, 4423−4432.
20. Liu, Y., Nesheim, J. C., Lee, S.-K., and Lipscomb, J. D. (1995) *J. Biol. Chem. 270*, 24662−24665.
21. Hendrich, M. P., Münck, E., Fox, B. G., and Lipscomb, J. D. (1990) *J. Am. Chem. Soc. 112*, 5861−5865.
22. Liu, K. E., Valentine, A. M., Wang, D. L., Huynh, B. H., Edmondson, D. E., Salifoglou, A., and Lippard, S. J. (1995) *J. Am. Chem. Soc. 117*, 10174−10185.
23. Liu, K. E., Valentine, A. M., Qiu, D., Edmondson, D. E., Appelman, E. H., Spiro, T. G., and Lippard, S. J. (1995) *J. Am. Chem. Soc. 117*, 4997−4998.
24. Shu, L., Nesheim, J. C., Kauffmann, K., Münck, E., Lipscomb, J. D., and Que, L., Jr. (1997) *Science 275*, 515−518.
25. Lee, S.-K., Fox, B. G., Froland, W. A., Lipscomb, J. D., and Münck, E. (1993) *J. Am. Chem. Soc. 115*, 6450−6451.
26. Liu, K. E., Wang, D., Huynh, B. H., Edmondson, D. E., Salifoglou, A., and Lippard, S. J. (1994) *J. Am. Chem. Soc. 116*, 7465−7466.
27. Fox, B. G., Liu, Y., Dege, J. E., and Lipscomb, J. D. (1991) *J. Biol. Chem. 266*, 540−550.
28. Pulver, S. C., Froland, W. A., Lipscomb, J. D., and Solomon, E. I. (1997) *J. Am. Chem. Soc. 119*, 387−395.

29. Liu, Y., Nesheim, J. C., Paulsen, K. E., Stankovich, M. T., and Lipscomb, J. D. (1997) *Biochemistry 36*, 5223−5233.
30. Paulsen, K. E., Liu, Y., Fox, B. G., Lipscomb, J. D., Münck, E., and Stankovich, M. T. (1994) *Biochemistry 33*, 713−722.
31. Froland, W. A., Andersson, K. K., Lee, S.-K., Liu, Y., and Lipscomb, J. D. (1992) *J. Biol. Chem. 267*, 17588−17597.
32. Chang, S. L., Wallar, B. J., Lipscomb, J. D., and Mayo, K. H. (1999) *Biochemistry 38*, 5799−5812.
33. Rosenzweig, A. C., Brandstetter, H., Whittington, D. A., Nordlund, P., Lippard, S. J., and Frederick, C. A. (1997) *Proteins 29*, 141−152.
34. Walters, K. J., Gassner, G. T., Lippard, S. J., and Wagner, G. (1999) *Proc. Natl. Acad. Sci. U.S.A. 96*, 7877−7882.
35. Lloyd, J. S., Bhambra, A., Murrell, J. C., and Dalton, H. (1997) *Eur. J. Biochem. 248*, 72−79.
36. Brandstetter, H., Whittington, D. A., Lippard, S. J., and Frederick, C. A. (1999) *Chem. Biol. 6*, 441−449.
37. Fox, B. G., Froland, W. A., Jollie, D. R., and Lipscomb, J. D. (1990) *Methods Enzymol. 188*, 191−202.
38. Shriver, Z., Hu, Y., and Sasisekharan, R. (1998) *J. Biol. Chem. 273*, 10160−10167.
39. Lundblad, R. L. (1994) *Techniques in Protein Modification*, pp 105−128, CRC Press, Boca Raton, FL.
40. Cardy, D. L., Laidler, V., Salmond, G. P., and Murrell, J. C. (1991) *Mol. Microbiol. 5*, 335−342.
41. McDonald, I. R., Uchiyama, H., Kambe, S., Yagi, O., and Murrell, J. C. (1997) *Appl. Environ. Microbiol. 63*, 1898−1904.
42. Shinohara, Y., Uchiyama, H., Yagi, O., and Kusukabe, I. (1998) *J. Ferment. Bioeng. 85*, 37−42.
43. Grosse, S., Laramee, L., Wendlandt, K. D., McDonald, I. R., Miguez, C. B., and Kleber, H. P. (1999) *Appl. Environ. Microbiol. 65*, 3929−3935.
44. Stainthorpe, A. C., Lees, V., Salmond, G. P., Dalton, H., and Murrell, J. C. (1990) *Gene 91*, 27−34.
45. Brazeau, B. J., and Lipscomb, J. D. (2000) *Biochemistry 39*, 13503−13515.
46. Valentine, A. M., Stahl, S. S., and Lippard, S. J. (1999) *J. Am. Chem. Soc. 121*, 3876−3887.
47. Tyson, C. A., Lipscomb, J. D., and Gunsalus, I. C. (1972) *J. Biol. Chem. 247*, 5777−5784.
48. Gunsalus, I. C., Meeks, J. R., Lipscomb, J. D., Marshall, V. P., Debrunner, P. G., and Münck, E. (1974) in *Molecular Mechanisms of Oxygen Activation* (Hayaishi, O., Ed.) pp 561−613, Academic Press, New York.
49. Newman, L. M., and Wackett, L. P. (1995) *Biochemistry 34*, 14066−14076.
50. Pikus, J. D., Studts, J. M., Achim, C., Kauffmann, K. E., Münck, E., Steffan, R. J., McClay, K., and Fox, B. G. (1996) *Biochemistry 35*, 9106−9119.
51. Pikus, J. D., Mitchell, K. H., Studts, J. M., McClay, K., Steffan, R. J., and Fox, B. G. (2000) *Biochemistry 39*, 791−799.
52. Whited, G. M., and Gibson, D. T. (1991) *J. Bacteriol. 173*, 3010−3016.
53. Qian, H., Edlund, U., Powlowski, J., Shingler, V., and Sethson, I. (1997) *Biochemistry 36*, 495−504.
54. Cadieux, E., and Powlowski, J. (1999) *Biochemistry 38*, 10714−10722.
55. Small, F. J., and Ensign, S. A. (1997) *J. Biol. Chem. 272*, 24913−24920.
56. Miura, A., and Dalton, H. (1995) *Biosci., Biotechnol., Biochem. 59*, 853−859.
57. Green, J., and Dalton, H. (1985) *J. Biol. Chem. 260*, 15795−15801.
58. Shu, L., Liu, Y., Lipscomb, J. D., and Que, L., Jr. (1996) *J. Biol. Inorg. Chem. 1*, 297−304.

BI002298B